ChemPhysChem

Research Article
doi.org/10.1002/cphc.202300561

Chemistry Europe
European Chemical Societies Publishing

www.chemphyschem.org

Increasing Complexity in Adamantyl Thioethers Characterized by Rotational Spectroscopy

Pablo Pinacho,*[a, b] Donatella Loru,[a] Tatjana Šumanovac,[c] Marina Šekutor,*[c] and Melanie Schnell*[a, d]

We report on the synthesis and characterization using high-resolution rotational spectroscopy of three bulky thioethers that feature an adamantyl group connected to a sulfur atom. Detailed experimental and theoretical structures are provided and compared with the 1,1′-diadamantyl ether. In addition, we expand on previous findings concerning microsolvation of adamantyl derivatives by investigating the cluster formation between these thioethers and a water molecule. The investigation of such clusters provides valuable insights into the sulfur-centered hydrogen bonding in thioethers with increasing size and steric repulsion.

Introduction

The role of sulfur in biological processes cannot be overstated. From its ubiquitous presence in living organisms, including linking of polypeptide strands in proteins *via* a disulfide bond between two cystein residues, to the importance in structures of natural products and pharmaceuticals,[1] sulfur is an essential element of life irreplaceable in cell biology. Moreover, the sulfur atom provides unique properties and biochemical pathways to the pharmaceuticals. For example, the usefulness of sulfur-containing peptides in drug discovery is reflected in improved stability and pharmacokinetic profiles of such compounds.[2] Apart from its presence in the building blocks of life, sulfur is also often contained in agrochemicals[3] and in materials, from rubber vulcanization to batteries manufacture.[4] In drug design, the thioether group (R–S–R′) is of special importance; thioethers can be found both in linear and cyclic moieties of bioactive molecules.[5,6] Additionally, thioethers are common starting points in the formation of higher oxidation state sulfur derivatives, both synthetically[7] and in nature.[8]

Other molecular scaffolds that impart unique properties based on their distinctive structure are diamondoids. They are characterized by a high symmetry of their cage skeletons, as exemplified by adamantane, the smallest diamondoid.[9–12] Introduction of the adamantyl group into more complex molecular systems adds structural stability, while its bulkiness and lipophilicity influence their chemical properties. The discovery of antiviral activity of amantadine, the primary amine of adamantane,[13] initiated a new research direction in medicinal chemistry. In a relatively short time, a plethora of adamantyl derivatives were described, showing antiviral, antibacterial, and/or antiparkinson activity, among others.[10] Adamantyl derivatives are used in targeted drug delivery, material science, as well as being investigated in an astrochemical context.[10,14–18] Despite a vast number of prepared derivatives, a combination of the adamantyl group with thioethers remains scarcely described in the literature. Some notable recent examples include 1-adamantyl methyl thioether[19,20] as well as a nickel(I) complex with 1-adamantyl methyl thioether containing substituents,[21] 1-adamantyl ethyl thioether,[22] and 1,1′-diadamantyl thioether.[23,24]

Alkyl adamantyl thioethers have a great potential as new pharmaceuticals due to the combination of special properties emerging from both functional groups. To obtain a deep understanding of their physico-chemical properties, it is crucial to have a good description of their molecular structure. Adamantane and its derivatives have been extensively characterized using various techniques, including nuclear magnetic resonance (NMR),[25] infrared spectroscopy (IR) of both neutral and cationic species,[26,27] as well as IR or electronic photodissociation spectroscopy.[17,18] One of the most accurate methodologies to determine experimental structures of molecules and complexes in the gas phase is rotational spectroscopy.[28] With modern broadband rotational spectrometers using a supersonic expansion, a high spectral resolution can be achieved, and transitions from very similar isomers,

[a] Dr. P. Pinacho, Dr. D. Loru, Prof. Dr. M. Schnell
Deutsches Elektronen-Synchrotron DESY
Notkestr. 85, 22607 Hamburg (Germany)

[b] Dr. P. Pinacho
Present address: Physical Chemistry Department
University of the Basque Country (UPV/EHU)
B° Sarriena, S/N, 48940, Leioa (Spain)
E-mail: pablo.pinacho@ehu.eus

[c] Dr. T. Šumanovac, Dr. M. Šekutor
Department of Organic Chemistry and Biochemistry
Ruđer Bošković Institute
Bijenička cesta 54, 10000 Zagreb (Croatia)
E-mail: msekutor@irb.hr

[d] Prof. Dr. M. Schnell
Christian-Albrechts-Universität zu Kiel
Institute of Physical Chemistry
Max-Eyth-Str. 1, 24118 Kiel (Germany)
E-mail: melanie.schnell@desy.de

Supporting information for this article is available on the WWW under https://doi.org/10.1002/cphc.202300561

conformers, and isotopologues can be discriminated.[29–31] The expansion cools down the rotational degrees of freedom and creates an isolated environment, where the molecules can be probed to analyze their inherent structures and interactions. Additionally, the supersonic expansion grants the generation of many-body complexes, allowing for the study of a number of molecular species in the same experiment.[32–34]

Using broadband rotational spectroscopy, we previously studied 1,1′-diadamantyl ether (DAE) and its complexes with solvent molecules.[35,36] DAE is a good model to analyze the interplay between London dispersion and hydrogen bonding interactions; it possesses two adamantyl groups that are good dispersion energy donors as well as a linking ether group that is in turn a good hydrogen bond acceptor. By investigating DAE complexes with different solvents, we were able to directly observe how the size and polarity of the solvent molecules subtly affect the formation and stability of the complexes. Exploring these subtle effects enhances our comprehension of the interplay between hydrogen bonding (a directional force) and dispersion interactions (a weaker but cumulative force) within a given system. Gained insights into the fundamental nature of intermolecular interactions also have practical implications for the molecular design, since accurate prediction of these effects often reveals key supramolecular driving forces in (bio)chemical processes.

In this work, we study three alkyl adamantyl thioethers of increasing size and complexity. By exchanging the oxygen atom of DAE with sulfur in the analogues, we retain the main molecular geometry while significantly modifying physical and chemical properties. Our main objective is to characterize the emerging effects induced by this substitution. Additionally, these compounds serve as excellent models to describe the sulfur-water interactions, or sulfur-centered hydrogen bonds (SCHB) in general. Sulfur is usually thought to be involved in weak interactions, at the limit of what can be described as hydrogen bonding. The capability of sulfur to establish hydrogen bonding networks in thiols (R–SH) in the gas phase using FTMW spectroscopy has previously been studied in detail.[37–39] However, SCHB in other sulfur derivatives such as thioethers has not been so extensively investigated. Recent examples include the characterization of microsolvated complexes of diethyl disulfide and dimethyl sulfide.[40,41] The investigation of the monohydrated complexes for the three selected sulfur-adamantane compounds can therefore provide valuable insight into the capability of sulfur to act as hydrogen bond acceptor in such systems.

Results and Discussion

The molecules studied herein are showcased in Figure 1. They feature an adamantyl group attached to a sulfur atom and a varying alkyl group of increasing size as the other substituent. Specifically, the molecules are 1-adamantyl methyl thioether ($C_{11}H_{18}S$, AMT) with the smallest alkyl group, followed by 1-adamantyl *tert*-butyl thioether ($C_{14}H_{24}S$, ATT), and the bulkiest 1,1′-diadamantyl thioether ($C_{20}H_{30}S$, DAT).

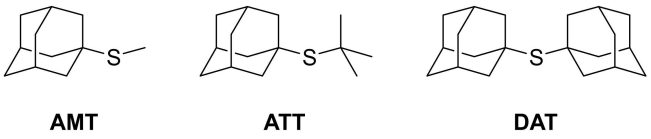

Figure 1. Structures of 1-adamantyl methyl thioether (AMT), 1-adamantyl tert-butyl thioether (ATT), and 1,1′-diadamantyl thioether (DAT).

The three thioethers feature a quite rigid structure with the bulky adamantyl groups. Therefore, only one conformation is expected for each of them. We confirmed this by performing a conformational search using the CREST code,[42] which resulted in a single minimum structure, with the geometries shown in Figure 2. Because of the presence of a single conformer, the assignment of the broadband rotational spectra of the monomers was straightforward. All molecules in the series exhibit intense patterns of rotational transitions (Figures S1–S3), which could be easily assigned to the monomers of AMT, ATT and DAT (Figure 2). The rotational transitions in AMT show a characteristic splitting attributed to the internal rotation of the methyl top (S–CH_3) which was analyzed to determine the experimental value of the internal rotation barrier (V_3). No splitting patterns were observed for any other species. The experimental rotational parameters determined for the three molecules are summarized in Table 1. The intensity of the transitions in AMT and ATT was sufficient to detect all the ^{13}C and the ^{34}S isotopologues in their natural abundance (approximately 1.1% and 4%, respectively, rotational constants in Tables S1–S2), which allowed to determine the r_s and the r_0 experimental structures. AMT contains a symmetry plane which divides the adamantyl group in two halves, with the equivalent carbon atoms on either side of the plane (Figure S4). As a result, the spectra of the singly-substituted ^{13}C isotopologues of these carbon atoms are identical, effectively doubling their relative intensity (Table S1). For DAT, the S/N ratio of the spectrum was not sufficient for the observation of its ^{13}C isotopologues. However, considering the good agreement between the experimental and theoretical spectroscopic parameters (Table 1), it is justified to rely the analysis of the structure on theoretical r_e values.

The r_s method is based on solving the Kraitchman's equations[43] to determine the coordinates of each atom from the change in the moments of inertia upon isotopic substitution. The Kraitchman method provides only the absolute value for the coordinates, and the signs are usually taken from theoretical calculations. In the other approach, the r_0 method,[44] a least-squares fit of the molecular structure is performed using the UNEX software package,[45] to reproduce the experimental rotational constants in the ground vibrational state.[46] The initial geometries for the r_0 fit were taken from the computations at the B3LYP-D3(BJ)/def2-TZVP level of theory. Both methods (r_s and r_0) provide valuable information about the molecular structure, they can be applied independently of each other, and each of them has some advantages and drawbacks. The predicted r_e and the experimental r_s structures of the three

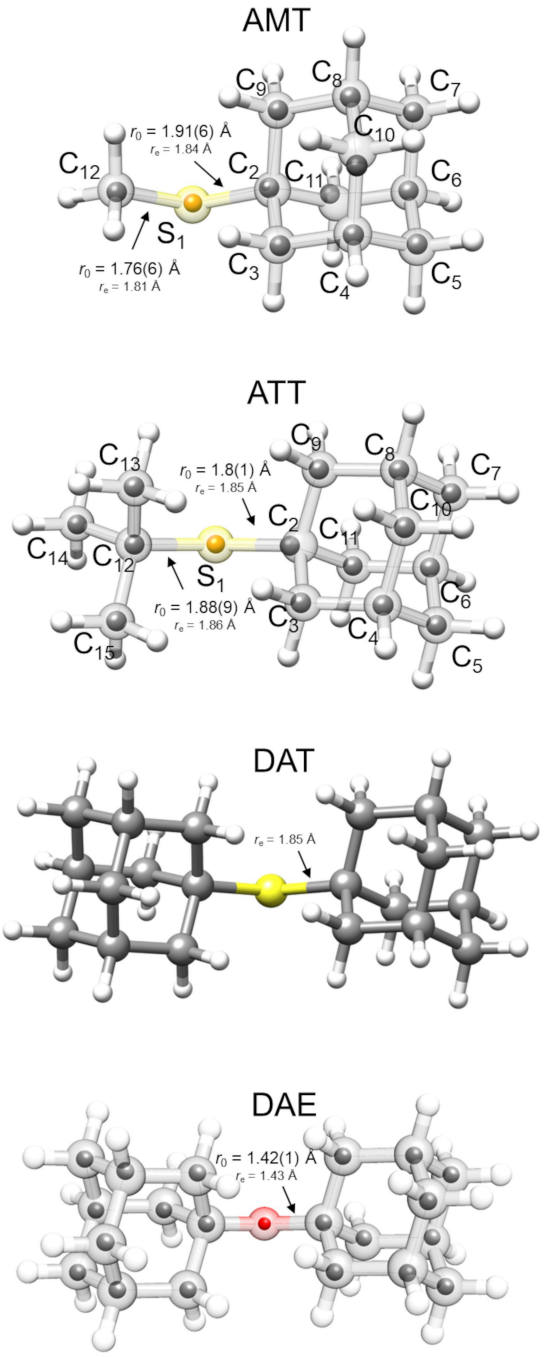

Figure 2. Experimental r_s structure for AMT and ATT (inner solid grey spheres) and theoretical (B3LYP-D3(BJ)/def2-TZVP) r_e structure (outer semi-transparent balls). It was not possible to determine the r_s for DAT, and the structure analysis relies on the r_e. The experimental structure for DAE from reference 35 is given for comparison.

monomers are shown in Figure 2, while the most relevant structural parameters are presented in Table 2.

Figure 2 presents the theoretical structure of DAT as well as the experimental structure of 1,1′-diadamantyl ether (DAE), the oxygen analogue of DAT. The substitution of oxygen by sulfur leads to an increase in the ether/thioether bond length and a decrease in the C_2—O/S—C_{12} angle (Table 2). A Non-Covalent Interaction (NCI) analysis has been performed to visualize the intramolecular interactions in these molecules (Figure 3). The scatter graphs for the NCI analysis are shown in Figure S5 in the SI. As the substituent size increases, dispersion interactions become more prominent. For the largest molecules, DAE and DAT, the NCI surfaces reveal interactions of similar shape and strength despite the substitution of the oxygen atom with sulfur.

As previously mentioned, the observed splitting in the AMT transitions was attributed to the internal rotation motion of the S–CH_3 top (Figure S6). Analysis of the splitting resulted in the determination of the rotational constants and the barrier height (V_3) for the motion. The experimental value of 513.60(21) cm^{-1} is well reproduced by the theoretical computations (507 cm^{-1}) and falls within the range of other methyl sulfide molecules reported in the literature.[47,48] The longer bond distance in the S–CH_3 molecules results in smaller V_3 values than the oxygen compounds for almost all the thioethers, as reported in the literature.[49]

The next step was the analysis of the monohydrated complexes to explore the formation of hydrogen bonds and extend previous studies about SCHB. The conformational search using theoretical methods resulted in one low-energy conformation for each of the thioethers. The three complexes show a similar interaction network, in which the water molecule acts as the hydrogen bond donor and the sulfur atom as the acceptor (Figure 3). High-energy isomers for the monohydrated complexes were predicted, in which the water molecule interacts solely with hydrogen atoms of the adamantyl and the alkyl groups. Those structures were disregarded due to their high relative energies of about 20 $kJ \cdot mol^{-1}$. For the stable microsolvated complexes, we performed geometry optimizations, as well as NCI and SAPT calculations. The theoretical spectroscopic parameters were used to simulate the rotational spectra and aid the search for the monohydrated species in the experimental spectra. The residual water in the gas bottle and in the gas lines was sufficient to enable the formation and spectral identification of the water complexes with 1-adamantyl methyl thioether (AMT-w) and 1-adamantyl *tert*-butyl thioether (ATT-w). However, to observe the monohydrated complex of 1,1′-diadamantyl thioether (DAT-w) it was necessary to repeat the experiment with additional water in an external reservoir. The determined spectroscopic parameters and the observed intensities of the transitions show an excellent agreement with the theoretical rotational constants and the predicted values of the dipole-moment components, which allowed an unambiguous assignment for each of the complexes (Table 3). Only few transitions exhibit the splitting expected from the internal rotation of the S–CH_3 top for the AMT-w. Due to their low intensity, it was not possible to analyze the splitting pattern in more detail to determine the V_3 barrier for the complex.

In all the three monohydrated complexes, the theoretical O_w—H_w···S distance is predicted to be only slightly longer than the equivalent distance H_w···O in the DAE-w cluster.[35] Likewise, the O_w—H_w···O/S angle is similar in all cases (Table S3). The NCI analysis reveals that the O_w—H_w···S hydrogen bond is of moderate strength with some additional O_w···H—C dispersion interactions, which become more important as the size of the

Table 1. Experimental and theoretical (B3LYP-D3(BJ)/def2-TZVP) spectroscopic constants for the AMT, ATT, and DAT monomers. The final fit for AMT was achieved using the XIAM program, while SPFIT was used for ATT and DAT.

	AMT		ATT		DAT	
	Experimental	Theoretical	Experimental	Theoretical	Experimental	Theoretical
A (MHz)[a]	1526.989(35)[b]	1531.1	1144.26486(23)	1145.8	743.793721(85)	743.6
B (MHz)	669.400(25)	667.3	358.387422(62)	358.1	172.596201(60)	172.7
C (MHz)	645.864(24)	643.5	350.936979(61)	350.4	168.062925(62)	168.0
D_J (kHz)	0.0097(24)	–	0.00503(20)[c]	–	0.00153(11)[c]	–
D_{JK} (kHz)	0.0566(32)	–	0.00822(61)	–	–	–
D_K (kHz)	–	–	0.0521(71)	–	–	–
d_1(kHz)	0.00110(63)	–	–	–	–	–
d_2 (kHz)	−0.00052(14)	–	–	–	–	–
V_3 (cm^{-1})	513.60(21)	507	–	–	–	–
V_3 ($kJ \cdot mol^{-1}$)	6.1439(26)	6.1	–	–	–	–
$\mu_a/\mu_b/\mu_c$ (D)	Y/Y/N	−1.1/1.3/0.0	Y/Y/N	−0.6/−1.4/0.0	N/Y/N	0.0/−1.6/0.0
N	251	–	311		222	–
σ (kHz)	10.9	–	6.5		6.4	–

[a] A, B, and C are the rotational constants; D_J, D_{JK}, D_K, d_1, and d_2 are the quartic centrifugal distortion constants. V_3 is the barrier height for the internal rotation of the methyl top. μ_a, μ_b, and μ_c are the electric dipole-moment components of the transitions (N: not observed, Y: observed). N is the number of fitted transitions. σ is the root-mean square deviation of the fit. [b] Standard error in parentheses in units of the last digit. [c] For ATT and DAT, the A-reduction was used, therefore the quartic centrifugal distortion constants are Δ_J, Δ_{JK}, and Δ_K.

Table 2. Selected experimental (r_s and r_0) and theoretical (r_e, B3LYP-D3(BJ)/def2-TZVP) bond distances (Å) and angles (°) for AMT, ATT, DAT, and DAE. Atom labelling presented in Figure 2.

	AMT			ATT			DAT	DAE		
	r_0	r_s	r_e	r_0	r_s	r_e	r_e	r_0[a]	r_s[b]	r_e
O/S_1–C_2	1.91(6)	1.87(2)	1.84	1.8(1)	1.673(2)	1.85	1.85	1.42(1)	–	1.43
O/S_1–C_{12}	1.76(6)	1.804(3)	1.81	1.88(9)	1.831(6)	1.86	1.85	1.42(1)	–	1.43
C_{12}–O/S_1–C_{12}	103(3)	98(17)	117.7	111(6)	100.1(2)	111.8	112.	127.2(0.9)	–	127

[a] From reference 35. [b] For DAE, the ^{18}O isotopologue was not observed.

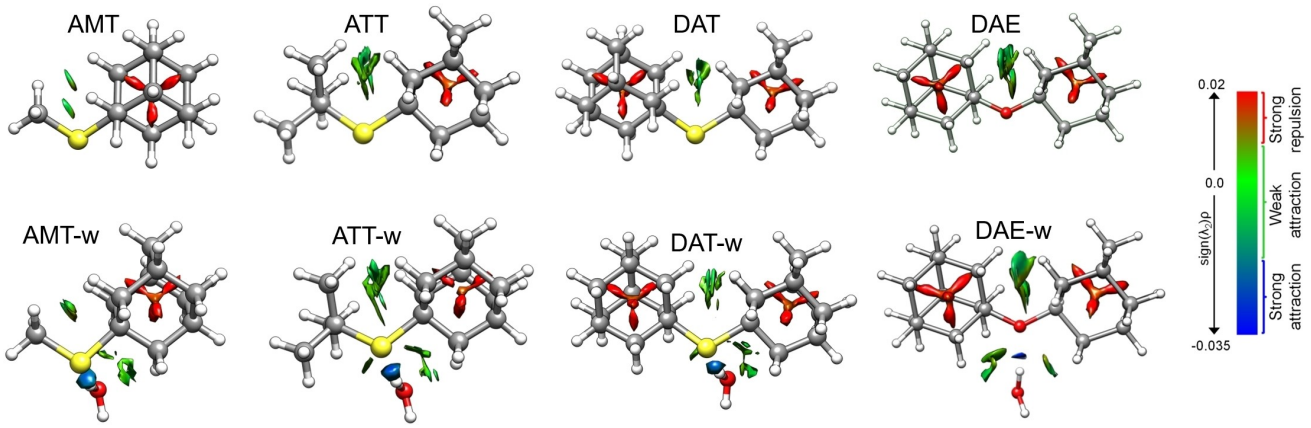

Figure 3. Structures of the monomers AMT, ATT, DAT, and DAE together with their monohydrated complexes AMT-w, ATT-w, DAT-w, and DAE-w. The NCI are plotted using a cut-off value for the isosurface of 0.5 for all the molecules and complexes discussed. The strength of the interaction depends on the value and sign of λ_2. The blue color appearing in the hydrogen bonds represent strong attractive forces. Green surfaces represents weak attractive interactions, like dispersion, and appear between C–H···H–C or C–H···O. The red areas inside the bulky adamantyl substituents indicate strong repulsive interactions.

Table 3. Experimental and theoretical (B3LYP-D3(BJ)/def2-TZVP) spectroscopic constants for the AMT-w, ATT-w, and DAT-w complexes. The final fits were achieved using SPFIT.

	AMT-w		ATT-w		DAT-w	
	Experimental	Theoretical	Experimental	Theoretical	Experimental	Theoretical
A (MHz)[a]	1024.8474(11)[b]	1037.2	777.67811(46)	774.9	535.36043(35)	546.3
B (MHz)	558.00146(80)	559.7	333.12541(14)	342.6	169.36432(11)	168.8
C (MHz)	480.67462(84)	485.1	295.62125(13)	303.0	156.448285(59)	157.1
Δ_J (kHz)	0.048(13)	-	0.00685(67)	-	-	-
Δ_{JK} (kHz)	-	-	0.0555(91)	-	0.0229(25)	-
Δ_K (kHz)	0.555(68)	-	-	-	0.0364(53)	-
δ_J (kHz)	-	-	-	-	-	-
δ_K (kHz)	-	-	-	-	-	-
$\mu_a/\mu_b/\mu_c$ (D)	Y/Y/N	-1.0/-1.4/-0.3	Y/Y/N	0.5/1.5/-0.4	N/Y/N	-0.5/-1.4/-0.5
N	26	-	57		111	-
σ (kHz)	7.0	-	4.2		6.8	-

[a] Parameter definitions in Table 1. [b] Standard error in parentheses in units of the last digit.

group increases. The same conclusion was reached in the case of DAE complexes with solvents of different size, as the dispersion forces increased with the size.[35]

Symmetry-Adapted Perturbation Theory (SAPT) computations at the SAPT2+/jun-cc-pVDZ level were performed to obtain information of the interaction energy of the monohydrated complexes. An additional gain from SAPT computations is the decomposition of the total energy into the electrostatic, induction, dispersion, and exchange components. The total energy follows an increasing trend with the size of the alkyl group that is consistent with the NCI analysis (Table 4). As the substituent becomes larger, the percentage of electrostatic and induction contributions to the stability of the complex decreases, while the percentage of dispersion increases. This result highlights the importance of dispersion interaction to the net stability as the substituent increases. The SAPT computation for DAE-w at the same level gives higher values for all the contributions than for the sulfur analogue, illustrating the capacity of oxygen to form more stable interactions. The interaction energies were also calculated at the B3LYP-D3(BJ)/def2-TZVP level of theory considering the Basis Set Superposition Error (BSSE). These computations result in higher energies compared to the SAPT values (Table 4). However, the same increasing tendency with the substituent size can be observed.

Table 4. Symmetry-Adapted Perturbation Theory energy (SAPT2+/jun-cc-pVDZ) and contributions of the electrostatic, dispersion, induction and repulsion forces for AMT-w, ATT-w, DAT-w, and DAE-w. The interaction energy for each complex is also calculated considering the basis set superposition error (BSSE) at the B3LYP-D3(BJ)/def2-TZVP level of theory. All the energies in $kJ \cdot mol^{-1}$.

SAPT interaction energy	AMT-w	ATT-w	DAT-w	DAE-w
Electrostatic	-40.9	-44.3	-44.6	-57.4
Exchange	52.3	58.1	59.0	73.4
Induction	-14.8	-16.2	-16.3	-19.2
Dispersion	-15.2	-18.1	-19.4	-23.1
Total	-18.6	-20.5	-21.3	-26.4
% Electrostatic[a]	57.7	56.4	55.5	57.6
% Induction	20.9	20.6	20.3	19.3
% Dispersion	21.4	23.0	24.2	23.2
Interaction energy (BSSE)	-26.4	-28.9	-29.6	-30.7

[a] Percentage relative to the sum of the attractive forces (electrostatic, induction, and dispersion).

The fact that the three thioethers AMT, ATT, and DAT, along with the oxygen analogue DAE, form identical hydrogen bond patterns highlights the stability of that disposition for the molecule of water. It is important to emphasize that complexation with water does not change the structure of the thioethers, *i.e.*, the bond distances and angles of the monomers remain unaltered upon complexation as observed for DAE-w (Table S3).

Conclusions

A series of adamantyl thioether derivatives with increasing size and complexity has been synthesized and studied by high-resolution rotational spectroscopy. Furthermore, we observed their microsolvated complexes with one molecule of water. Precise experimental structures were determined for the smaller monomers, AMT and ATT. For the remaining structures, structural analysis relied on theoretical computations in combination with the rotational spectroscopy results. Comparison of DAT and DAE shows that a change of oxygen to a larger sulfur atom modifies slightly the structure of the monomer, while the interaction site of water in the complexes is similar in both cases. The behavior of water in the smaller derivatives was found to be comparable, providing insight into the preference

of water to establish hydrogen bonds with thioethers. We analyzed the splitting generated by the rotation of a methyl top in the smaller compound, AMT, and compared it with other S–CH_3 molecules reported. The determined barrier for the motion of the methyl top in AMT falls within the range of values for alkyl thioethers. In all the examined cases, the S–CH_3 barriers were lower than the corresponding O–CH_3 counterparts. Lastly, it should be remarked that 1,1′-diadamantyl thioether (DAT) is one of the largest molecules studied to date by high-resolution rotational spectroscopy, highlighting the challenges for measurement and analysis of large size compounds.

Experimental Section and Computational Details

Synthesis of thioethers

All ^{1}H and ^{13}C NMR spectra were recorded with a Bruker AV-600 NMR spectrometer, and the NMR spectra were referenced to the residual proton or carbon signal of the used deuterated solvent as an internal standard (Figures S7–S9). IR spectra were recorded with FT IR-ATR Perkin Elmer UATR. GC-MS analyses were performed on an Agilent 7890B/5977B GC/MSD instrument equipped with a HP-5 ms column. All solvents were obtained from commercial sources and used without further purification.

Synthesis of 1-adamantyl methyl thioether[22] **(AMT)**: Na (0.23 g, 0.01 mmol) was dissolved in absolute methanol (20 mL) and 1-adamantanethiol[22] (1.0 g, 0.006 mol) and MeI (0.63 mL, 0.01 mol) were added. The reaction mixture was refluxed for 1 h and after cooling to room temperature, the solvent was evaporated under reduced pressure to 1/3 of the initial volume and then *n*-hexane (50 mL) was added. Layers were separated in a separating funnel and the methanol layer was extracted with *n*-hexane (2×50 mL). Combined *n*-hexane layers were dried over Na_2SO_4, filtered, and evaporated to produce 1.0 g (92%) of the colorless oily product. The resulting crude product was purified by column chromatography using *n*-hexane as the eluent, yielding DAT as a colorless oil (0.443 g, 73%). ^{1}H NMR (600 MHz, $CDCl_3$), $\delta = 1.65–1.73$ (m, 6H), 1.84 (d, 6H, $J = 2.4$ Hz), 2.0 (s, 3H), 2.03–2.06 (m, 3H) ppm. ^{13}C NMR (150 MHz, $CDCl_3$), $\delta = 8.8$, 29.6, 36.4, 42.7, 42.8 ppm. MS (EI) *m/z*: 182.1 (M^+). IR (neat), $\tilde{\nu}_{max} = 2902$ (s), 2848 (s), 1450 (m), 1342 (m), 1046 (w) cm^{-1}.

Synthesis of 1-adamantyl *tert*-butyl thioether (ATT): 1-Adamantanethiol[22] (0.3 g, 1.8 mmol) was dissolved in *tert*-butanol (20 mL) and 2 mL of conc. sulfuric acid was added. The reaction mixture was heated at 40 °C for 24 h in a sealed tube. After cooling to room temperature, 50 mL of *n*-hexane was added, the reaction mixture was transferred to a separating funnel and washed with saturated aqueous solution of $NaHCO_3$ (50 mL). The aqueous layer was extracted with *n*-hexane (2×50 mL) and the combined organic layers were dried over Na_2SO_4. After filtration and evaporation of the solvent under reduced pressure, 0.394 g (98%) of a colorless waxy solid was obtained. According to the GC-MS analysis the solid was a mixture of 15% of 1-adamantanethiole and 85% of the desired product. Column chromatography using *n*-hexane as the eluent gave 0.265 g (66%) of ATT as a colorless waxy solid and 0.066 g (16%) of the starting 1-adamantanethiole. ^{1}H NMR (600 MHz, $CDCl_3$), $\delta = 1.43$ (s, 9H), 1.68–1.71 (m, 6H), 2.00–2.05 (m, 9H) ppm. ^{13}C NMR (150 MHz, $CDCl_3$), $\delta = 30.0$, 33.7, 36.4, 45.3, 46.1, 48.6 ppm. MS (EI) *m/z*: 224.3 (M^+). IR (neat), $\tilde{\nu}_{max} = 2958$ (w), 2903 (s), 2849 (s), 1471 (w), 1452 (m), 1359 (m), 1342 (w), 1302 (w), 1161 (m), 1101 (w), 1041 (m), 684 (w) cm^{-1}.

Synthesis of 1,1′-diadamantyl thioether[23] **(DAT)**: 1-adamantylmethanesulfonate[50] (0.460 g, 2 mmol), 1-adamantanethiol[22] (0.336 g, 2 mmol) and TEA (0.28 mL, 2 mmol) were heated in a sealed tube at 100 °C for 48 h. The reaction mixture was cooled to room temperature and dissolved in CH_2Cl_2 (10 mL), extracted with water (10 mL) and washed with 5% H_2SO_4 (aq.) (10 mL) and Na_2CO_3 (sat., aq.) (10 mL). The organic phase was dried over Na_2SO_4, filtered and evaporated. The resulting crude product was purified by column chromatography (0→100% CH_2Cl_2/*n*-hexane as the eluent), yielding DAT as a white solid (0.443 g, 73%). M.p. 231–232 °C (lit.[23] 231.0–231.5 °C). ^{1}H NMR (600 MHz, $CDCl_3$), $\delta = 1.69$ (br. s, 12H), 2.00 (br. s, 6H), 2.05–2.10 (m, 12H) ppm. ^{13}C NMR (150 MHz, $CDCl_3$), $\delta = 30.1$, 36.4, 45.9, 49.3 ppm. MS (EI) *m/z*: 302.3 (M^+). IR (neat), $\tilde{\nu}_{max} = 2899$ (s), 2886 (s), 2847 (s), 1447 (m), 1342 (m), 1295 (m), 1035 (s), 814 (w), 686 (w) cm^{-1}.

Chirped-pulse Fourier transform microwave (CP-FTMW) spectroscopy

The spectra were recorded with the broadband chirped-pulse Fourier-transform microwave (CP-FTMW) spectrometer COMPACT in the frequency range 2–8 GHz in Hamburg.[30] Different conditions were used for each of the samples, but the general procedure is as follows. The samples were held in a reservoir inside a vacuum chamber and heated (60 °C for AMT, 130 °C for ATT, and 180 °C for DAT) to generate sufficient vapor pressure. The sample vapor was diluted in Ne as carrier gas, with a backing pressure of 1–2 bars. We used a pulsed valve with a repetition rate of 8 Hz to supersonically expand the gas mixture into the vacuum chamber, where it formed a macroscopic polarization induced by a 4 μs microwave chirp pulse. The microwave pulses were created by an arbitrary waveform generator (AWG), amplified by a traveling wave tube amplifier (300 W of power), and broadcasted into the chamber by a horn antenna. The free induction decay (FID) of the macroscopic polarization was recorded in the time domain using an oscilloscope. The Fast Fourier transformation of the FID provided the spectrum in the frequency domain. A fast frame setup was used, which allowed to probe each supersonic expansion with eight back-to-back excitation pulses,[51] thus reducing measurement time and sample consumption. A total of 4.1 million averages were collected in the experiments for AMT, ATT, and DAT. The intensity of the transitions for AMT and ATT was sufficient to observe the singly substituted ^{13}C and ^{34}S isotopologues in natural abundance, along with the monohydrated complexes. The signal to noise ratio (SNR) for AMT was measured to be of 1100 for some of the most prominent transitions in the experimental spectrum. For its monohydrated cluster, the SNR was around 13. The SNR for the most intense transitions of ATT was of about 1200, while its water cluster, ATT-w, had a SNR around 13 for the most intense transitions. The relatively low intensity of the rotational spectrum of DAT (SNR around 90 for the most intense transitions) did not enable the observation of any rare isotopologue or water complex. The monohydrated cluster of DAT was investigated by performing a second experiment in which a reservoir containing water, external to the vacuum chamber, was added to the gas line. The experimental conditions were optimized to favor water complexation, this involved heating the internal reservoir containing DAT up to 185 °C and using neon at a backing pressure of 3 bars. The final spectrum was recorded by averaging 3.4 million acquisitions, and the most intense transitions of DAT-w reached a SNR of 40. All the spectra feature line resolution of *ca.* 25 kHz and accuracy in the frequency measurement better than 15 kHz.

A preliminary fit of the species was obtained using an asymmetric rigid rotor Hamiltonian in the JB95 software.[52] Refined fits for ATT, DAT, and their complexes with water were obtained using the A-reduction, I^r representation semirigid rotor Hamiltonian implemented in the SPFIT program.[53] The final fit for AMT was performed using Watson's S-reduction implemented in XIAM to analyze the splitting due to the internal rotation of the methyl top.[54] The final fit for the AMT-w complex was obtained using the A-reduction, I^r representation with SPFIT.

Computational Details

We explored the conformational landscape of monomers and complexes using the CREST code[42] based on GFN2-xTB.[55,56] Structure optimizations using the B3LYP-D3(BJ)[57,58] dispersion-corrected functional with the def2-TZVP[59] basis set were performed within the harmonic approximation to obtain zero-point corrected relative energies using the ORCA program package, version 5.0.[60,61] Energy scans to compute the barrier for the internal rotation motion were all performed at the B3LYP-D3(BJ)/def2-TZVP level of theory using ORCA version 5.0.

The weak intra- and intermolecular forces were identified by a Non-Covalent Interactions (NCI) analysis.[62,63] The sign of λ_2 from the NCI calculations is associated with the nature and strength of the interaction. Positive values of λ_2 indicate repulsive interactions, while negative values depict stronger NCI forces. Values of λ_2 close to zero indicate the presence of weak attractive interactions, such as van der Waals forces. To generate the NCI surfaces the Multiwfn[64] software was used, while Chimera[65] was employed for its visualization. For the monohydrated clusters, Symmetry-Adapted Perturbation Theory (SAPT)[66] computations (SAPT2+ with the jun-cc-pVDZ basis set) were also performed to obtain the interaction energy of the complex and decompose it into its components using the PSI4 package.[67] Additionally, BSSE-corrected energies were obtained using the counterpoise method at the B3LYP-D3(BJ)/def2-TZVP level of theory.

Acknowledgements

We thank Dr. D. Tikhonov for scientific discussion. We acknowledge financial support from the Croatian Science Foundation (project UIP-2017-05-9653 "Diamondoid scaffolds containing heteroatoms – preparation and application in development of advanced materials"), and from the COST Action CA21101 "Confined molecular systems: From a new generation of materials to the stars" (COSY) supported by COST (European Cooperation in Science and Technology). Parts of the computations were performed by using the European XFEL and DESY funded Maxwell computational resources operated at Deutsches Elektronen-Synchrotron DESY, Hamburg, Germany, and the resources of the computer cluster Isabella based in SRCE – University of Zagreb, University Computing Centre. P.P. acknowledges a Maria Zambrano grant (UPV/EHU, Ministry of Universities, Recovery, Transformation, and Resilience Plan – Funded by the European Union – Next Generation EU, MAZAM22/16). Open Access funding enabled and organized by Projekt DEAL.

Conflict of Interests

The authors declare no conflict of interest.

Data Availability Statement

The data that support the findings of this study are available from the corresponding author upon reasonable request.

Keywords: thioether · sulfur-centered hydrogen bond · adamantyl derivatives · non-covalent interactions · rotational spectroscopy

[1] B. R. Beno, K.-S. Yeung, M. D. Bartberger, L. D. Pennington, N. A. Meanwell, *J. Med. Chem.* **2015**, *58*, 4383–4438.
[2] J. Zhao, X. Jiang, *Chin. Chem. Lett.* **2018**, *29*, 1079–1087.
[3] P. Devendar, G.-F. Yang, *Top. Curr. Chem.* **2017**, *375*, 82.
[4] D. A. Boyd, *Angew. Chem. Int. Ed.* **2016**, *55*, 15486–15502.
[5] E. A. Ilardi, E. Vitaku, J. T. Njardarson, *J. Med. Chem.* **2014**, *57*, 2832–2842.
[6] K. A. Scott, J. T. Njardarson, *Top. Curr. Chem.* **2018**, *376*, 5.
[7] X. B. Liu, Q. Rong, J. Tan, C. Chen, Y. L. Hu, *Front. Chem.* **2022**, *9*, 798603.
[8] Z. Rao, X. Li, Y.-G. Fang, J. S. Francisco, C. Zhu, C. Chu, *J. Am. Chem. Soc.* **2023**, *145*, 10839–10846.
[9] R. C. Fort Jr., *Adamantane – The Chemistry of Diamond Molecules*, Marcel Dekker: New York **1976**.
[10] L. Wanka, K. Iqbal, P. R. Schreiner, *Chem. Rev.* **2013**, *113*, 3516–3604.
[11] H. Schwertfeger, A. A. Fokin, P. R. Schreiner, *Angew. Chem. Int. Ed.* **2008**, *47*, 1022–1036.
[12] M. A. Gunawan, J.-C. Hierso, D. Poinsot, A. A. Fokin, N. A. Fokina, B. A. Tkachenko, P. R. Schreiner, *New J. Chem.* **2014**, *38*, 28–41.
[13] W. L. Davies, R. R. Grunert, R. F. Haff, J. W. McGahen, E. M. Neumayer, M. Paulshock, J. C. Watts, T. R. Wood, E. C. Hermann, C. E. Hoffmann, *Science* **1964**, *144*, 862.
[14] A. Štimac, M. Šekutor, K. Mlinarić-Majerski, L. Frkanec, R. Frkanec, *Molecules* **2017**, *22*, 297.
[15] J. Liu, D. Obando, V. Liao, T. Lifa, R. Codd, *Eur. J. Med. Chem.* **2011**, *46*, 1949–1963.
[16] K. Spilovska, F. Zemek, J. Korabecny, E. Nepovimova, O. Soukup, M. Windisch, K. Kuca, *Curr. Med. Chem.* **2016**, *23*, 3245–3266.
[17] M. A. R. George, O. Dopfer, *Chem. Eur. J.* **2022**, *28*, e20220057.
[18] P. B. Crandall, D. Müller, J. Leroux, M. Förstel, O. Dopfer, *Astrophys. Lett.* **2020**, *900*, L20.
[19] L. Melzig, C. R. Diene, C. J. Rohbogner, P. Knochel, *Org. Lett.* **2011**, *13*, 3174–3177.
[20] E. Alfonzo, S. M. Hande, *Org. Lett.* **2021**, *23*, 6115–6120.
[21] K. Fujita, A. L. Rheingold, C. G. Riordan, *Dalton Trans.* **2003**, 2004–2008.
[22] K. K. Khullar, L. Bauer, *J. Org. Chem.* **1971**, *36*, 3038–3040.
[23] I. Akhrem, A. Orlinkov, S. Vitt, *Inorg. Chim. Acta* **1998**, *280*, 355–359.
[24] G. F. Pavelko, *Journal of Friction and Wear* **2012**, *33*, 443–452.
[25] R. C. Fort Jr, P. von R. Schleyer, *J. Org. Chem.* **1965**, *30*, 789–796.
[26] R. Mecke, R. Spiesecke, *Chem. Ber.* **1955**, *88*, 1997–2002.
[27] A. Patzer, M. Schutz, T. Möller, O. Dopfer, *Angew. Chem. Int. Ed.* **2012**, *51*, 4925–4929.
[28] W. Gordy, R. L. Cook, *Microwave Molecular Spectra*, Vol. 11, Wiley Interscience, New York **1984**.
[29] S. R. Domingos, C. Pérez, C. Medcraft, P. Pinacho, M. Schnell, *Phys. Chem. Chem. Phys.* **2016**, *18*, 16682–16689.
[30] D. Schmitz, V. Alvin Shubert, T. Betz, M. Schnell, *J. Mol. Spectrosc.* **2012**, *280*, 77–84.
[31] J. L. Alonso, J. C. López, *Top. Curr. Chem.* **2015**, *364*, 335–401.
[32] D. R. Miller, *Atomic and Molecular Beam Methods* ed. G. Scoles, Oxford University press, Oxford **1988**, Volume 1.
[33] H. Singh, P. Pinacho, D. A. Obenchain, M. M. Quesada-Moreno, M. Schnell, *Phys. Chem. Chem. Phys.* **2022**, *24*, 27312–27320.
[34] R. S. Ruoff, T. D. Klots, T. Emilsson, H. S. Gutowsky, *J. Chem. Phys.* **1990**, *93*, 3142–3150.
[35] M. M. Quesada-Moreno, P. Pinacho, C. Pérez, M. Šekutor, P. R. Schreiner, M. Schnell, *Chem. Eur. J.* **2020**, *26*, 10817–10825.

[36] M. M. Quesada-Moreno, P. Pinacho, C. Pérez, M. Šekutor, P. R. Schreiner, M. Schnell, *Chem. Eur. J.* **2021**, *27*, 6198–6203.
[37] M. Juanes, A. Lesarri, R. Pinacho, E. Charro, J. E. Rubio, L. Enríquez, M. Jaraiz, *Chem. Eur. J.* **2018**, *24*, 6564–6571.
[38] M. Juanes, R. T. Saragi, R. Pinacho, J. E. Rubio, A. Lesarri, *Phys. Chem. Chem. Phys.* **2020**, *22*, 12412–12421.
[39] R. T. Saragi, M. Juanes, C. Pérez, P. Pinacho, D. S. Tikhonov, W. Caminati, M. Schnell, A. Lesarri, *J. Phys. Chem. Lett.* **2021**, *12*, 1367–1373.
[40] X. Li, T. Lu, D. A. Obenchain, J. Zhang, S. Herbers, J.-U. Grabow, G. Feng, *Angew. Chem. Int. Ed.* **2020**, *133*, 5902–5906.
[41] T. Lu, J. Zhang, Y. Xu, Z. Wang, G. Feng, Z. Zeng, *Spectrochim. Acta Part A* **2023**, *288*, 122199.
[42] P. Pracht, F. Bohle, S. Grimme, *Phys. Chem. Chem. Phys.* **2020**, *22*, 7169–7192.
[43] J. Kraitchman, *Am. J. Phys.* **1953**, *21*, 17–24.
[44] H. D. Rudolph, *Struct. Chem.* **1991**, *2*, 581–588.
[45] Y. V. Vishnevskiy, UNEX 1.7 **2023**. https://unex.vishnevskiy.group (accessed Mon Sep 04 2023).
[46] Z. Kisiel, *J. Mol. Spectrosc.* **2003**, *218*, 58–67.
[47] M. Hayashi, M. Adachi, J. Nakagawa, *J. Mol. Spectrosc.* **1981**, *86*, 129–135.
[48] A. Jabri, V. Van, H. V. L. Nguyen, H. Mouhib, F. Kwabia Tchana, L. Manceron, W. Stahl, I. Kleiner, *Astron. Astrophys.* **2016**, *589*, A127.
[49] L. Tulimat, H. Mouhib, H. V. L. Nguyen, W. Stahl, *J. Mol. Spectrosc.* **2020**, *373*, 111356.
[50] R. K. Crossland, K. L. Servis, *J. Org. Chem.* **1970**, *35*, 3195.
[51] C. Pérez, S. Lobsiger, N. A. Seifert, D. P. Zaleski, B. Temelso, G. C. Shields, Z. Kisiel, B. H. Pate, *Chem. Phys. Lett.* **2013**, *571*, 1–15.
[52] D. Plusquellic, JB95, available at http://www.nist.gov/pml/electromagnetics/grp05/jb95.cfm.
[53] H. M. Pickett, *J. Mol. Spectrosc.* **1991**, *148*, 371–377.
[54] H. Hartwig, H. Dreizler, *Z. Naturforsch. A* **1996**, *51*, 923–932.
[55] S. Grimme, C. Bannwarth, P. Shushkov, *J. Comput. Theory Chem.* **2017**, *13*, 1989–2009.
[56] C. Bannwarth, S. Ehlert, S. Grimme, *J. Chem. Theory Comput.* **2019**, *15(3)*, 1652–1671.
[57] a) C. Lee, W. Yang, R. G. Parr, *Phys. Rev. B* **1988**, *37*, 785–789; b) A. D. Becke, *J. Chem. Phys.* **1993**, *98*, 5648–5652; c) S. H. Vosko, L. Wilk, M. Nusair, *Can. J. Phys.* **1980**, *58*, 1200–1211.
[58] S. Grimme, J. Antony, S. Ehrlich, H. Krieg, *J. Chem. Phys.* **2010**, *132*, 154101.
[59] a) F. Weigend, R. Ahlrichs, *Phys. Chem. Chem. Phys.* **2005**, *7*, 3297–3305; b) F. Weigend, *Phys. Chem. Chem. Phys.* **2006**, *8*, 1057–1065.
[60] F. Neese, *Wiley Interdiscip. Rev.: Comput. Mol. Sci.* **2012**, *2*, 73–78.
[61] F. Neese, *Wiley Interdiscip. Rev.: Comput. Mol. Sci.* **2022**, *12*, e1606.
[62] E. R. Johnson, S. Keinan, P. Mori-Sánchez, J. Contreras-García, A. J. Cohen, W. Yang, *J. Am. Chem. Soc.* **2010**, *132*, 6498–6506.
[63] J. Contreras-García, E. R. Johnson, S. Keinan, R. Chaudret, J. P. Piquemal, D. N. Beratan, W. Yang, *J. Chem. Theory Comput.* **2011**, *7*, 625–632.
[64] T. Lu, F. Chen, *J. Comput. Chem.* **2012**, *33*, 580–592.
[65] E. F. Pettersen, T. D. Goddard, C. C. Huang, G. S. Couch, D. M. Greenblatt, E. C. Meng, T. E. Ferrin, *J. Comput. Chem.* **2004**, *25*, 1605–1612.
[66] B. Jeziorski, R. Moszynski, K. Szalewicz, *Chem. Rev.* **1994**, *94*, 1887–1930.
[67] R. M. Parrish, L. A. Burns, D. G. A. Smith, A. C. Simmonett, A. E. DePrince, E. G. Hohenstein, U. Bozkaya, A. Y. Sokolov, R. D. Remigio, R. M. Richard, J. F. Gonthier, A. M. James, H. R. McAlexander, A. Kumar, M. Saitow, X. Wang, B. P. Pritchard, P. Verma, H. F. Schaefer, K. Patkowski, R. A. King, E. F. Valeev, F. A. Evangelista, J. M. Turney, T. D. Crawford, C. D. Sherrill, *J. Chem. Theory Comput.* **2017**, *13*, 3185–3197.

Manuscript received: August 8, 2023
Revised manuscript received: September 4, 2023
Accepted manuscript online: September 6, 2023
Version of record online: October 9, 2023